The Physics of Nuclear Spin Systems

Furkan Selim Cetin

17/12/24

Abstract

Spin physics is essential for some of the greatest advancements in modern medicine, and science as a whole. The invention and continued use of Nuclear Magnetic Resonance (NMR) Imaging (MRI) relies entirely on our understanding of nuclear spin systems. The introduction of MRI as a standard imaging technique available almost everywhere in the world has allowed for unprecedented improvements in preventative and, by extension, curative medicine. This paper outlines the fundamental physics behind nuclear spin systems as used in NMR imaging.

List of Abbreviations

e.g. example given
EoM equation of motion
i.e. id est (*das heißt*)
MRI nuclear magnetic resonance imaging
NMR nuclear magnetic resonance
RF radio frequency
s.t. such that

Note that in the entirety of this paper, underlined variables $\underline{x}$ represent vectors or matrices, the hat symbol $\hat{x}$ implies an operator or a basis vector $\hat{e}_i$ of some coordinate system, and the wedge symbol $\wedge$ represents a vector cross product.

1 Introduction

In the 1920s, physicists observed unexplained patterns in atomic spectral lines, namely a splitting of the energy levels when applying an external magnetic field. The observed splitting further necessitated the existence of a degeneracy of the energy levels when there is no magnetic field being applied. This is illustrated in Figure 1.1. Following this discovery, one proposed solution was the concept of spin [1]. The discovery of spin physics led to huge advancements in modern medicine, such as NMR imaging, and in other areas of the natural sciences.

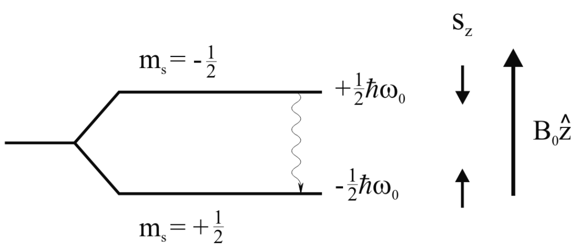

Figure 1.1: Zeeman splitting of a spin-$\frac{1}{2}$ system. [2]

1.1 Spin Statistics

Collections of different particles experience spin effects differently. This is generally referred to as the spin-statistics theorem. While integer-spin particles, namely bosons, follow Bose-Einstein Statistics, half-integer-spin particles, namely fermions, follow Fermi-Dirac Statistics. This is a consequence of the statistical nature of quantum mechanics, and its observed phenomena, such as the Pauli Exclusion Principle. The difference in the distribution functions of different particles is shown in Figure 1.2. The scope of this paper is limited to half-integer spin particles and the corresponding physics. More information on the Spin-Statistics Theorem can be found in Ref. [3].

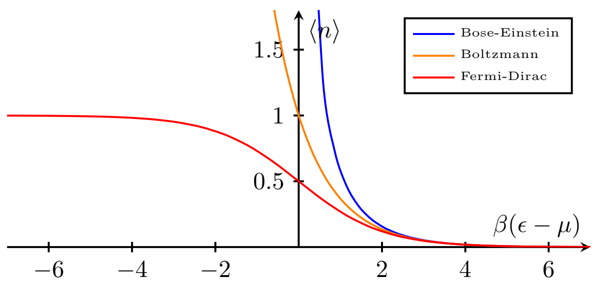

Figure 1.2: Average occupation number $\langle n \rangle$ of a quantum state as a function of the inverse temperature β and the energy ϵ. The orange graph depicts the classical Maxwell-Boltzmann Distribution. The blue and red graphs depict the distribution functions for a Bose-Einstein Distribution and a Fermi-Dirac Distribution, respectively.

2 Spin: Fundamentals

Spin is a fundamental quantum property of subatomic particles, which can be elementary or composite. It is independent of a particle's motion but can interact with motion-dependent quantities, such as momentum, and lead to observable effects, *e.g.* helicity effects. It can generally be visualised as an intrinsic type of angular momentum, since it also follows angular momentum rules of computation. It is, however, important to note that there is no classical analogue to spin. Particles behave as though they were spinning. They are associated with a magnetic moment $\underline{\mu}$, which allows them to interact with external magnetic fields, *e.g.* through precession. The nuclear spin of a hydrogen nucleus, depicted in Figure 2.1, in an applied magnetic field $\underline{B}_0$ precesses with some precessional frequency ω_0 [4].

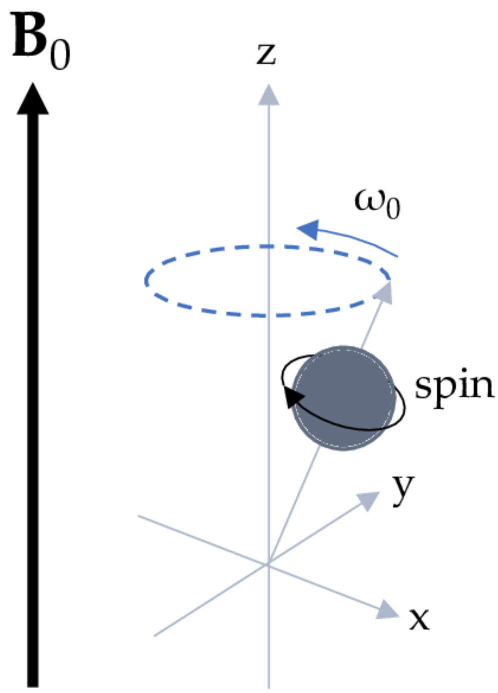

Figure 2.1: Nuclear spin of hydrogen in an applied field. [4]

2.1 Semi-Classical Approach

Spin is a quantum phenomenon, however it can be described using a semi-classical approach, only requiring the postulation of discretised, *i.e.* quantised, angular momenta and energies. The aim is to describe spin behaviour under an applied magnetic field $\underline{B}$. In the following, all magnetic fields $\underline{B}$ will be oriented along the z-axis, unless specified otherwise. The spins are treated as magnetic dipoles possessing a nuclear magnetic moment $\underline{\mu}$. Then, the angle between the magnetic moment and the magnetic field determines the energy of the state

$$E = -\underline{\mu} \cdot \underline{B} = \mu_z B_0 = -\hbar m \cdot \gamma B_0 = -\hbar\omega_0 m, \quad (2.1)$$

where μ_z is the z-component of $\underline{\mu}$, B_0 the magnetic field strength, γ the gyromagnetic ratio, and $\omega_0 \equiv \gamma B_0$ the Larmor frequency. Since the energy must be quantised, the angle can only take on discrete values, through the spin quantum number m. For a nucleus with spin number $I = \frac{1}{2}$, m can take on $\pm\frac{1}{2}$, *s.t.* there are two possible spin states. The states are referred to as spin-up and spin-down, for $m = +\frac{1}{2}$ and $m = -\frac{1}{2}$ respectively, with energies

$$E_{|\uparrow\rangle} = -\frac{1}{2}\hbar \cdot \gamma B_0 = -\frac{1}{2}\hbar \cdot \omega_0, \quad (2.2)$$

$$E_{|\downarrow\rangle} = +\frac{1}{2}\hbar \cdot \gamma B_0 = +\frac{1}{2}\hbar \cdot \omega_0. \quad (2.3)$$

State-down is the energetically higher state, and state-up the energetically cheaper state [5], as illustrated in Figure 2.2. It is also immediately apparent that the transitional energy of the two states is given by the Larmor frequency as well

$$\Delta E = E_{|\downarrow\rangle} - E_{|\uparrow\rangle} = \hbar\omega_0. \quad (2.4)$$

The energies, therefore, depend on the magnetic field strength B_0, *s.t.* this energy splitting collapses into a degeneracy at $B_0 = 0$, which is the observed phenomenon, and *s.t.* the transitional energy increases linearly with B_0 which is also observable.

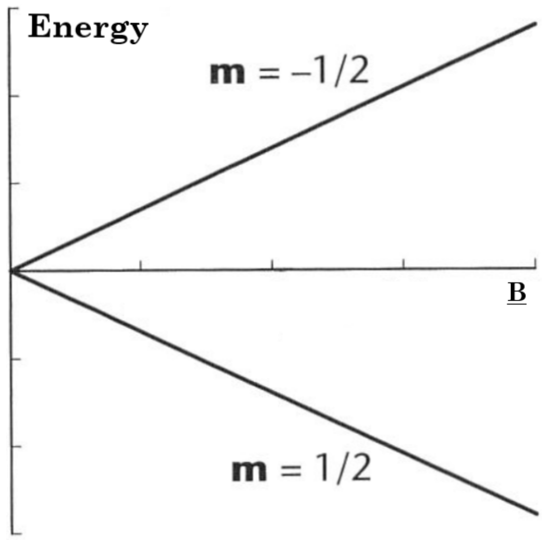

Figure 2.2: Energy splitting of nuclear spin levels of a spin-$\frac{1}{2}$ nucleus. Adapted from Ref. [5].

Furthermore, classically, the B field exerts a torque

$$\underline{\tau} = \underline{\mu} \wedge \underline{B} \quad (2.5)$$

on the magnetic dipole $\underline{\mu}$. The result of this applied torque is a top-like rotation of the magnetic moment around the applied field. This is called precession and it can be observed for spin as well. The spin states precess around the $\underline{B}$ field direction at Larmor frequency ω_0. Both eigenstates and the precessional motion of the ground state are depicted in Figure 2.3.

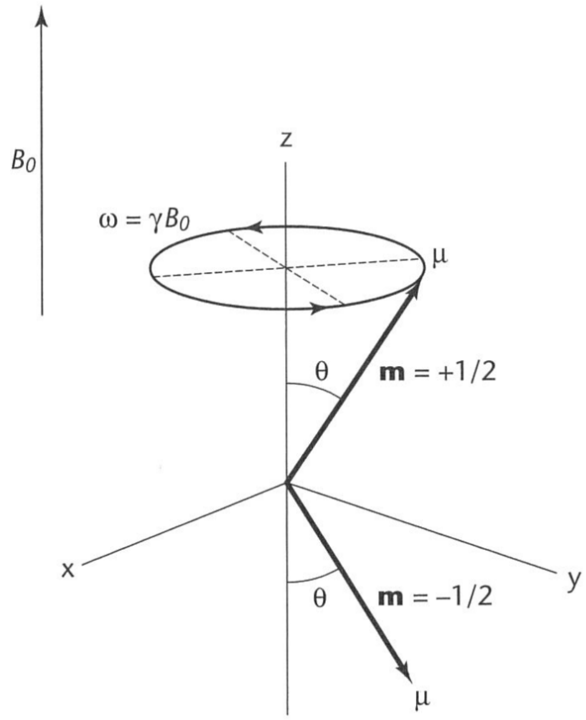

Figure 2.3: Precessional motion of the ground state of a spin-$\frac{1}{2}$ nucleus. [5]

Summarily, the energies of the states, the transitional energy between them, and the precessional motion are all determined by the Larmor frequency while the spin quantum number m discretises the energy as postulated [6].

2.2 Quantum Description of Spin

Since magnetism is a quantum mechanical effect, spin can also be described using a quantum description. Nuclear magnetism, in particular, is a pure spin magnetism, *s.t.* the magnetic moment operator

$$\hat{\mu} = \gamma \hat{I} \quad (2.6)$$

can be described by the spin operator $\hat{I}$. Moreover, spin operator eigenstates follow those of the angular momentum operator. With spin number I and spin quantum number m, the eigenvalues for some quantum state $|\psi\rangle$ are given by

$$\hat{I}^2 |\psi\rangle = \hbar^2 I(I+1) |\psi\rangle, \quad (2.7)$$

and

$$\hat{I}_z |\psi\rangle = \hbar m |\psi\rangle, \quad (2.8)$$

where m iterates from $-I$ to I in integer steps, resulting in $(2I+1)$ possible $\hat{I}_z$ spin states. Consequently, a nucleus with $I = 0$ will not exhibit any splitting of spin energy levels in a $\underline{B}$ field. For all nuclei $I \neq 0$, there will be at least two spin states, following the Zeeman splitting. Nuclei with $I > \frac{1}{2}$ have quadrupole moments and while such nuclei experience Zeeman splitting, *i.e.* a splitting of the spin energy levels in a magnetic field, they also experience a splitting of the spin energy levels in the presence of an electric field gradient, which leads to frequency shifts and relaxation effects. The frequency shifts are depicted in Figure 2.4, and show the introduction of some Δ to all transitions involving spin states $|m| > \frac{1}{2}$, as well as the consequences on the acquired signal, namely a noticeable shift in both directions. In order to circumvent this, only spin-$\frac{1}{2}$ nuclei will be further discussed. In the following, the considered nuclei all possess a spin $I = \frac{1}{2}$, and are thus described by the two-state model of up and down [7, 8].

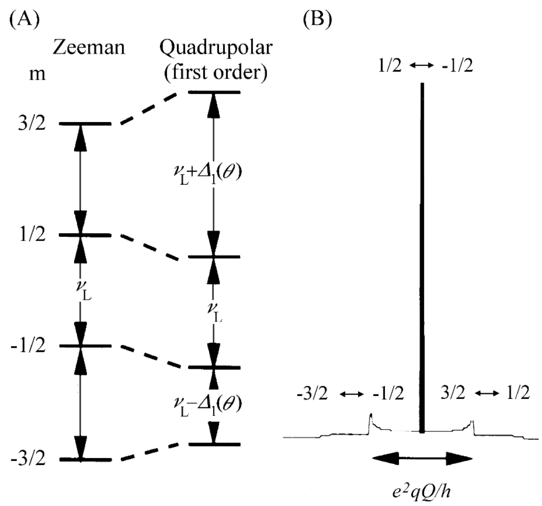

Figure 2.4: First-order frequency shift by perturbing electric field gradient. [9]

Considering a hydrogen nucleus with $I = \frac{1}{2}$, *i.e.* two possible spin states, an energy, and therefore also frequency, is associated with each spin state. In a vacuum, with no applied field, the spin states are degenerate and energetically equivalent. Therefore, the possible states are equally probable, and physically indistinguishable. No absorption or emission of energy is possible in this case. However, once a magnetic field $\underline{B} = B_0\hat{e}_z$ is applied, the spins precess around $\underline{B}$ with Larmor frequency ω_0 after some perturbation from their equilibrium position. The spin states are no longer degenerate, and are energetically non-equivalent, *i.e.* they have different energies. This splitting of spin energy levels, Zeeman splitting, is described by the Zeeman operator

$$\hat{H}_z |\psi\rangle = -\underline{\hat{\mu}}\underline{B} |\psi\rangle = -\underline{\hat{I}}\hat{e}_z\gamma B_0 |\psi\rangle = -\hat{I}_z\gamma B_0 |\psi\rangle$$

$$= -\hbar\gamma B_0 m |\psi\rangle = -\hbar\omega_0 m |\psi\rangle = E_m |\psi\rangle. \quad (2.9)$$

This is precisely the same result, as has been obtained using the semi-classical approach, in Equation 2.1

$$E = -\hbar\omega_0 m. \quad (2.10)$$

The two spin states, up and down, therefore have the same energies as in the semi-classical ansatz, given by Equation 2.2

$$E_{|\uparrow\rangle} = -\frac{1}{2}\hbar\omega_0 \quad (2.11)$$

and Equation 2.3

$$E_{|\downarrow\rangle} = +\frac{1}{2}\hbar\omega_0. \quad (2.12)$$

Transitions between the quantised spin states require absorption or emission of energy, as given in Equation 2.4

$$\Delta E = \hbar\omega_0. \quad (2.13)$$

The energetically cheaper state up is the ground state and is statistically more likely to be occupied than the energetically higher state down. This is visualised by the number of spins in both states in Figure 2.5.

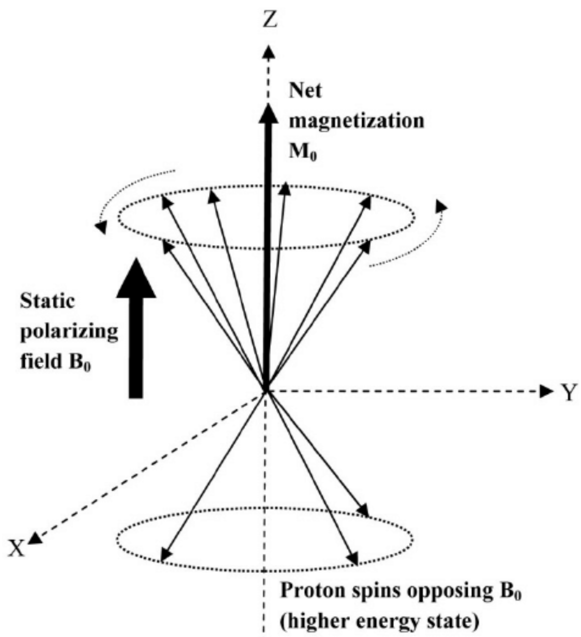

Figure 2.5: Precession of hydrogen nuclei around an applied field. The energetically higher state is in $-z$ direction and the energetically lower state in $+z$ direction, where the latter is more probable to be occupied. [10]

3 Spin Systems

Generally, it is not singular particles but collections of interacting particles in a spin ensemble that are observed and analysed. Such ensembles are referred to as spin systems. The ensemble or spin system consists of a large number of microscopic systems, the singular nuclear spins, which can occupy different microscopic states depending on the specific macroscopic conditions. The system is observed macroscopically, *i.e.* as a whole without focussing on individual particles. The spin system's statistical properties rely on that of the canonical ensemble.

The systems described in this section are collections of hydrogen nuclei, with nuclear spin $I = \frac{1}{2}$, *s.t.* there are two possible spin states, $m = \pm\frac{1}{2}$. The energy state populations are determined at thermal equilibrium, where lower energy states are more populated. Hence, state up is more populated than state down. The population difference is described by the Boltzmann distribution. At thermal equilibrium, the temperature T and the applied field B_0 determine how the states are populated

$$\frac{N_{|\downarrow\rangle}}{N_{|\uparrow\rangle}} = e^{-\beta\Delta E} = e^{-\frac{\hbar\omega_0}{k_B T}} \leq 1, \tag{3.1}$$

where k_B is the Boltzmann constant, and $\hbar$ the reduced Planck constant. Net absorption or emission of energy is only possible as long as there is a population difference, *i.e.*

$$\Delta N = N_{|\uparrow\rangle} - N_{|\downarrow\rangle} \neq 0. \tag{3.2}$$

Considering an ensemble generally consists of more than 10^{26} microsystems, *i.e.* nuclear spins, the difference in population numbers is very small with $\mathcal{O}(10^{-6})$, but nevertheless hugely important.

System perturbations, like radio frequency (rf) pulses, can lead to a diminishing ΔN,

$$\Delta N \to 0. \tag{3.3}$$

Following a perturbation, the population difference must be reestablished by relaxation. The relaxation processes are described in Section 3.3.

3.1 Magnetisation

Prior to continuing on with relaxation, it is necessary to introduce the magnetisation $\underline{M}$. It is a macroscopic observable that makes it possible to measure microscopic spin behaviour, since it is not feasible to observe individual spins in the context of an ensemble.

The net magnetisation represents the bulk magnetic properties of the spin system

$$\underline{M} = \frac{1}{V}\sum_i \underline{\mu}_i. \tag{3.4}$$

At thermal equilibrium, $\underline{M}$ is aligned with the applied field $\underline{B}_0 \parallel \underline{M} = M_0\hat{e}_z$. The magnetisation can be tipped away from its alignment by some perturbation, to initiate a precession around the applied field $\underline{B}_0$, at Larmor frequency ω_0.

The magnetisation can be separated into a longitudinal

$$\underline{M}_z = M_z\hat{e}_z \tag{3.5}$$

and a transverse

$$\underline{M}_\perp = M_x\hat{e}_x + M_y\hat{e}_y \tag{3.6}$$

component. At thermal equilibrium, the transverse magnetisation vanishes, and the longitudinal magnetisation is maximal [11, 12].

3.2 Rotating Reference Frame

The system can be further simplified by transitioning into a rotating reference frame S', thereby trivialising precessional motion. The rotating frame is set to rotate at precessional frequency ω_0, *s.t.* any magnetic moment $\underline{\mu}$ and magnetisation $\underline{M}$ in S' behave as if they were in a resting frame experiencing an effective magnetic field $\underline{B}_{eff}$ instead of the applied field $\underline{B}$.

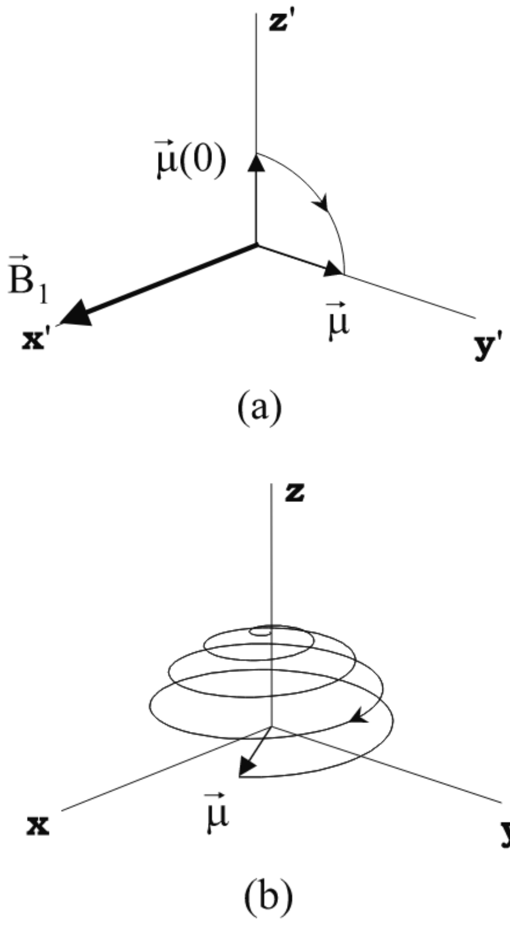

Figure 3.1: Effect of an rf pulse (90°_x) on a magnetic moment in (**a**) the rotating frame S', and (**b**) the lab frame S. [2]

In the rotating frame, a 90°_x pulse is immediately recognisable as such, and the magnetic moment's motion solely reflects the perturbation, as can be seen in

Figure 3.1. That same perturbation in the lab frame appears more complex because of the precessional rotation that occurs when the system is no longer in thermal equilibrium.

The remainder of this paper makes use of the simpler nature of the rotating frame and postulates its appropriateness, without deriving it. For more information, please note Refs. [2], [8], [13].

All variables are transformed into the rotating frame as required, while however maintaining the same notation.

3.3 Relaxation

Relaxation is necessary to reestablish the population difference that is present at thermal equilibrium, but diminishes with system perturbations, as discussed in the beginning of Section 3.

There are two types of relaxation that occur in spin systems, longitudinal relaxation and transverse relaxation. The information in this section can be found in Refs. [14, 6, 2].

T_1 Longitudinal Relaxation

Longitudinal relaxation is caused by spin-lattice interactions, where the lattice acts as a reservoir (in a canonical ensemble) and is able to absorb energy from the spin system without changing the system's temperature. This allows excited nuclei from higher energy states to return to the ground state. The longitudinal magnetisation decreases after a system perturbation, and returns to equilibrium through longitudinal relaxation. This process can be described by a simple differential equation

$$\frac{d}{dt}M_z = \frac{1}{T_1}(M_0 - M_z), \tag{3.7}$$

where M_z is the longitudinal magnetisation, M_0 the equilibrium magnetisation value, and T_1 the longitudinal relaxation time constant, responsible for scaling the relaxation process.

After some perturbation to the system that results in there only being transverse magnetisation $\underline{M}_\perp$, the longitudinal magnetisation M_z is reestablished by longitudinal relaxation, as shown in Figure 3.2. The time constant T_1 determines the time scale at which this occurs.

T_2 Transverse Relaxation

Transverse relaxation is caused by spin-spin interactions. Since every nuclear spin carries a magnetic moment, and thus generates a tiny magnetic field itself, no two spins experience the exact same field in the spin system. Spins experience so called local fields, which are a combination of the applied field and the fields of their neighbours. These variations in the local fields lead to the spins having differing precessional frequencies, since the frequency of precession is determined by the magnetic field that the spin experiences. Therefore, the spins dephase over time, because some spins precess faster than the Larmor frequency while some precess slower than the Larmor frequency.

Ultimately, the consequence of this is a decreasing net transverse magnetisation, which can be described by the differential equation

$$\frac{d}{dt}\underline{M}_\perp = -\frac{1}{T_2}\underline{M}_\perp, \tag{3.8}$$

where T_2 is the transverse relaxation time constant, which determines the time scale at which the dephasing occurs.

After some perturbation to the system, the net transverse magnetisation is maximal and immediately begins to dephase, as shown in Figure 3.3, until it vanishes. The transverse relaxation occurs at a much smaller time scale than longitudinal relaxation. In practice, often there are so-called micro fields and other B field inhomogeneities that reduce the time constant T_2 even further. Hence in reality, often times a constant T_2^* is used, where

$$T_2^* < T_2 < T_1. \tag{3.9}$$

Both of these relaxation processes play an important role in the following section, where the solutions to these differential equations will be discussed, as well as their significance in the time evolution of spin systems.

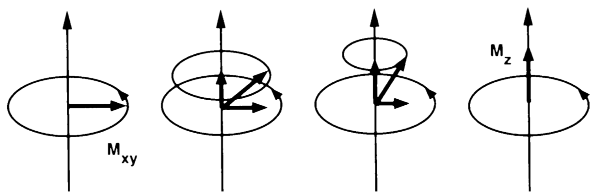

Figure 3.2: Schematic illustration of the T_1 relaxation process. Note that the process is depicted in the rotating frame. [11]

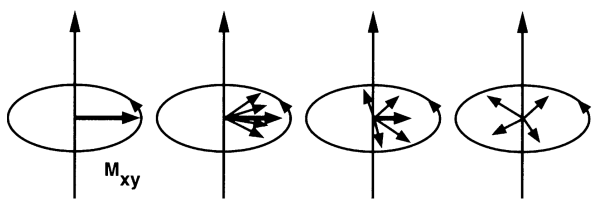

Figure 3.3: Schematic illustration of the T_2 relaxation process. Note that the process is depicted in the rotating frame. [11]

3.4 Spin Dynamics

Spin dynamics focusses on the time evolution of spin systems, considering both classical and quantum phenomena. The equation of motion (EoM) is given by the Bloch equation

$$\frac{d}{dt}\underline{M} = \underline{M} \wedge \gamma \underline{B}_{eff} + \frac{1}{T_1}(M_0 - M_z)\hat{e}_z - \frac{1}{T_2}\underline{M}_\perp. \quad (3.10)$$

The first term in the EoM is the classical term for the precessional motion, the second term describes the longitudinal recovery, and the third the spin dephasing and thus the decreasing net transverse magnetisation. The dynamics of a spin system after a 90°_x[1] rf pulse are illustrated in Figure 3.4. The rotation around the z axis is the precessional motion, the upwards direction is the result of T_1 and the decreasing radius in the transverse plane the result of T_2 relaxation. This is the process by which a spin system returns back to thermal equilibrium after a system perturbation [2].

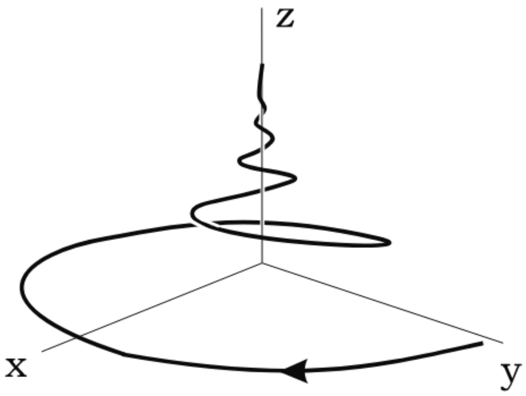

Figure 3.4: Illustration of the time evolution of the net magnetisation of a spin system following a 90°_x rf pulse. Note that the process is depicted in the laboratory rest frame. [2]

The dynamics are depicted in Figure 3.4, and are a graphical representation of the solution of the EoM. Generally, the solution can once again be separated into two distinct parts: the time evolution of the transverse and longitudinal magnetisation. The former is given by

$$\underline{M}_\perp(t) = \underline{M}_\perp(0)e^{-t/T_2}, \quad (3.11)$$

where $\underline{M}_\perp(0)$ is the initial transverse magnetisation immediately after the perturbation. This free induction decay is depicted in Figure 3.5 in both the lab and rotating frames. The longitudinal magnetisation is given by

$$M_z(t) = M_z(0)e^{-t/T_1} + M_0(1 - e^{-t/T_1}), \quad (3.12)$$

where $M_z(0)$ is the remaining longitudinal magnetisation after the perturbation and M_0 the equilibrium

[1] The subindex defines the rotation axis of the signal transformation caused by the rf pulse.

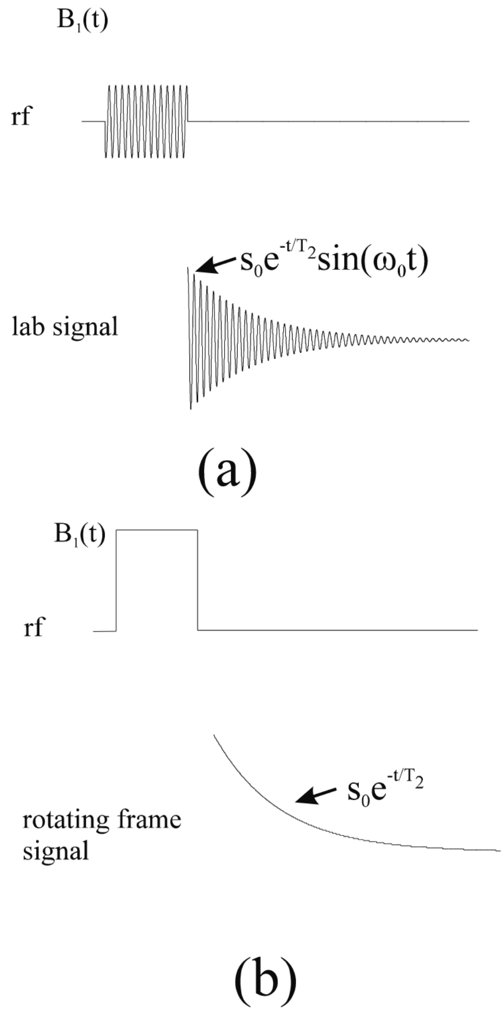

Figure 3.5: Illustration of the time evolution of the transverse magnetisation of a spin system following a 90°_x rf pulse. The process is depicted in both (**a**) the laboratory rest frame and (**b**) the rotating frame. Note that s_0 represents the signal amplitude and is essentially the absolute value of the magnetisation $\underline{M}_\perp(0)$. [2]

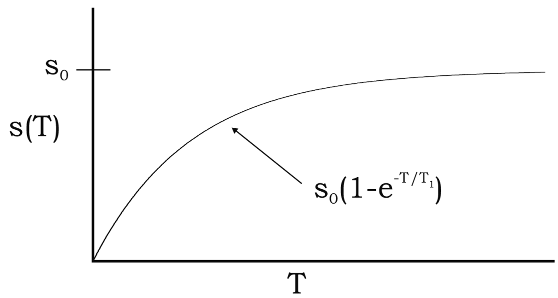

Figure 3.6: Illustration of the time evolution of the longitudinal magnetisation of a spin system following a 90°_x rf pulse, *s.t.* the perturbation flipped the entirety of the longitudinal magnetisation onto the transverse plane, *i.e.* $M_z(0) = 0$. Note that s_0 represents the signal amplitude and is essentially the equilibrium value of the magnetisation M_0. [2]

longitudinal magnetisation. This can be illustrated similarly to the transverse magnetisation, as shown in Figure 3.6.

4 Application: NMR Imaging

Nuclear magnetic resonance imaging (MRI) is one of the inventions that were made possible due to the discovery of and advancements in spin physics. MRI machines are used to create highly detailed images of soft tissue. It relies on the interactions of nuclear spins with an external magnetic field. While all nuclei $I \neq 0$ can, in principle, emit an acquirable signal, it is heavily dominated by hydrogen (^1H) nuclei, which account for more than 60% of the atoms in the human body.

4.1 Basic Design

An MRI machine consists of three distinct magnet layers with different properties, around some point where the patient is to be positioned. A schematic view of an MRI setup is shown in Figure 4.1.

The first and outermost magnet is the strongest of the three, providing a constant homogeneous field $\underline{B}_0$ in $\mathcal{O}(T)$. Its purpose is aligning the spins along the quantisation axis, *s.t.* a net longitudinal magnetisation is present. Moving to the middle layer, the gradient coils are used in such a way that allows for magnetic field gradients $\underline{G}$ to be generated along the three coordinate axes, independently of one another. The gradient fields, in $\mathcal{O}(mT)$, are necessary for spatial encoding of the image, which will be further discussed in Section 4.2. Lastly, the radio frequency coils, in $\mathcal{O}(\mu T)$, are designed to perturb the spin system through rf pulses, and to acquire the resulting signal.

The MRI signal acquisition process is illustrated in Figure 4.2. In the beginning, the strong magnetic field aligns the spins. Then, the system is perturbed by some rf pulse and the net magnetisation is flipped by

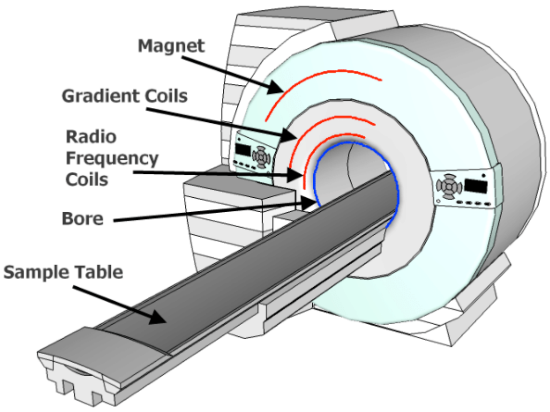

Figure 4.1: Schematic diagram of an MRI machine. [15]

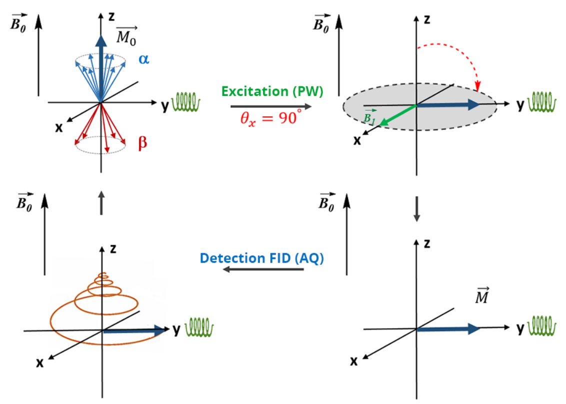

Figure 4.2: Schematic of the MRI signal acquisition process. [16]

a flip angle $\theta_x = 90°$. The resulting system possesses mainly transverse magnetisation, and immediately begins reestablishing equilibrium through relaxation processes, as discussed in Section 3.3. During this reestablishment, a signal can be acquired by the rf coils.

4.2 Spatial Encoding

In order to create an image, the information needs to be spatially encoded. The first step in this process is the slice selection (SS). A gradient G_z is applied in z direction, *s.t.* the Larmor frequency $\omega_0 = \omega_0(z)$ of the spins depends on their position along the respective axis. Meanwhile, an excitation rf pulse θ_x is generated. This pulse affects a certain bandwidth around a targeted frequency, where the Larmor equation applies. Thus, allowing the excitation of a transverse slice, as

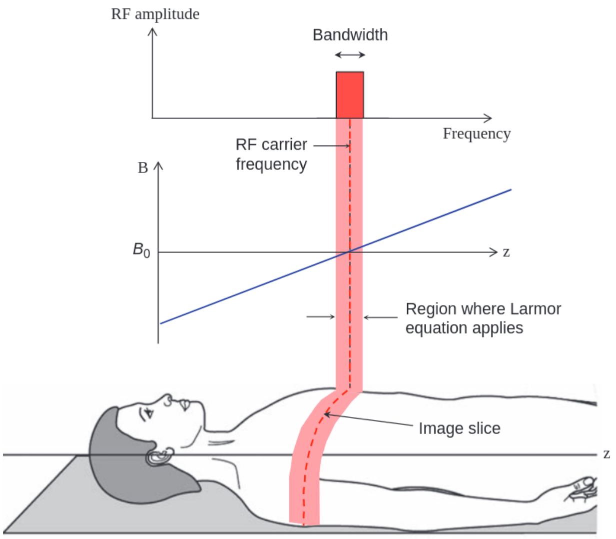

Figure 4.3: Selective slice selection of an image slice by applying an rf pulse and a gradient simultaneously. [6]

depicted in Figure 4.3, where the width of the slice depends on the magnitude of the gradient. Following SS, G_z is turned off again, and the excited slice must undergo phase encoding along the y axis. For this purpose, a gradient G_y is turned on for a short time period, which causes the precessional frequencies to differ depending on their y position, before it is turned off again. Now, the precessional frequencies return to the Larmor frequency, but with position-dependent phase changes. An illustrative example of this is shown in Figure 4.4 [6].

The final step is the frequency encoding of the x direction. This is done during signal acquisition, whereas the other two direction are encoded ahead of time. A gradient G_x is generated, *s.t.* the precessional frequencies become position dependent along the x direction, as shown in Figure 4.5. This allows for a complete encoding of an image, which can then be "decoded" via a Fourier Transform (FT).

Note that this is a drastic simplification of the spatial encoding process that is necessary to generate an image, which merely serves as a step-stone to understanding the basic principles of spatial encoding. For more information regarding spatial encoding, including resolution limitations, refer to Refs. [2], [6], [17].

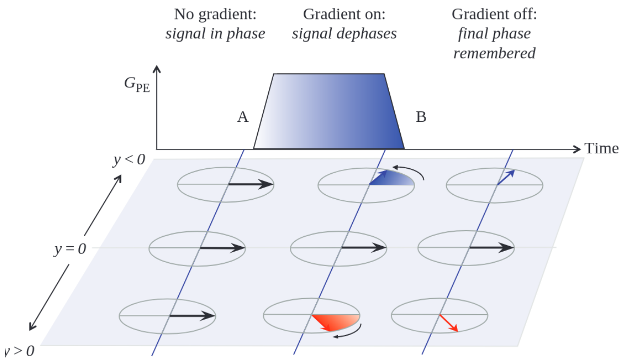

Figure 4.4: Phase encoding returns the signal to the Larmor frequency but with position-dependent phase changes. [6]

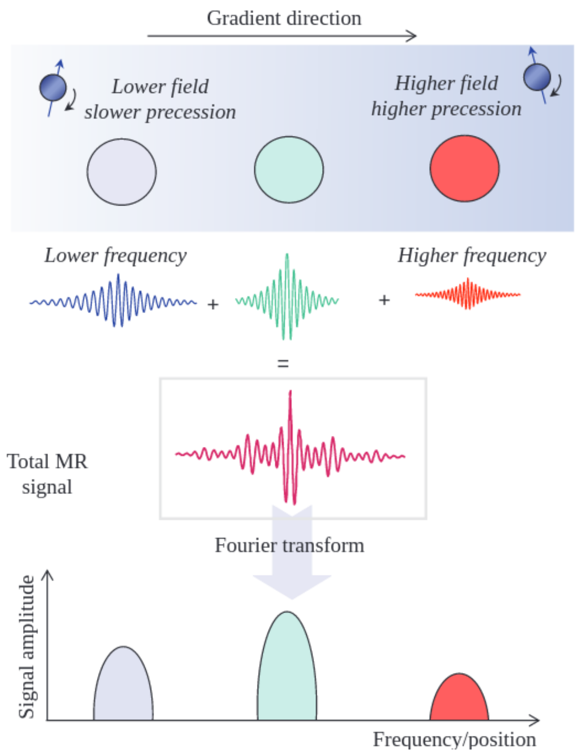

Figure 4.5: Frequency encoding description in terms of position-dependent frequency changes. [6]

4.3 Example: The Spin Echo Sequence

The spin-echo (SE) is one of several different imaging techniques that are used in MRI. The sequence is illustrated in Figure 4.6 and Figure 4.7.

First, a 90°_x pulse is applied, which flips the longitudinal magnetisation into the transverse plane. After the perturbation, the spins begin to dephase because of T_2 relaxation. Then, a 180°_y pulse is applied, which flips the (anti) clockwise rotating spins in such a way that they rephase into a singular direction corresponding to the initial peak. After rephasing to create the so-called echo the spins dephase again. The time between

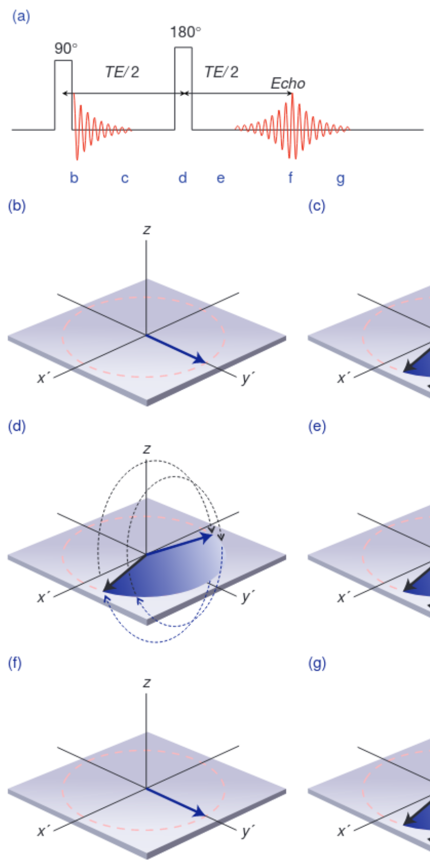

Figure 4.6: Spin-echo pulse sequence. [6]

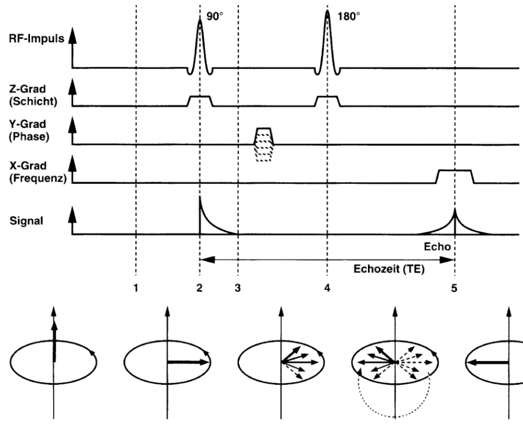

Figure 4.7: Frequency encoding description in terms of position-dependent frequency changes. Adapted from [11].

the two rf pulses determines the time of the signal echo. The time between the first and second rf pulse is defined as $TE/2$, whereas the echo occurs at the echo time TE, which marks the time between the first rf pulse and the echo.

4.4 Alternatives and Improvements to MRI?

The main reason, why MRI is as fundamentally established in modern medicine as it is, is that there are no viable alternatives for soft tissue imaging. Neither X-rays, nor CT images are able to deliver high fidelity images of soft tissue. An example of this is shown in Figure 4.8.

Furthermore, MRI does not require the use of ionising radiation, and is therefore far less invasive and destructive compared to other imaging techniques, while being able to provide images at much higher spatial resolution. There are certainly limitations to NMR imaging, such as bone imaging. Most practical limitations are based on the imaging process rather than the physics. MRI machines are expensive in all regards: the initial purchase, the maintenance, and the operation, which can unfortunately result in subpar medical care in terms of imaging in less economically developed countries. Furthermore, the imaging process takes quite long (around 30-60 mins), during which the patient must remain still. Taking the noise MRI machines create into consideration, some patients may find it difficult to stay still.

Since MRI machines require the patient to be placed inside of a cylindrical bore, the patient has to physically fit into the MRI machine to get imaged. Unfortunately, there have been several reports documenting cases where the physical size limitations or weight restrictions did not allow for patients to obtain the care they needed[2]. A case study from 2019 reports that over 40% of the cervical cancer patients, included in the report, were obese, while more than 14% were morbidly obese. The case study can be found in Ref. [20].

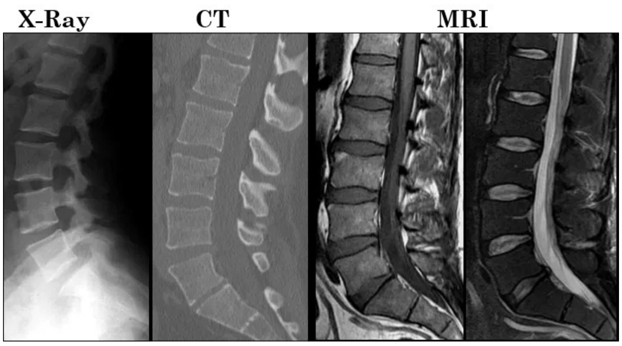

Figure 4.8: Comparison between images of the pelvis and spine using X-ray, CT, and MRI. Adapted from [18].

5 Conclusion

MRI technology has been immensely important in the advancement of modern medicine. It allows for non-invasive soft tissue imaging with high spatial resolution. Often patients had to undergo surgical procedures, in order to gain insight into soft tissue structures prior to the invention of MRI. While this imaging technique still poses challenges and limitations, just like any other, there are already several different techniques to improve upon regular MRI, such as *hyperpolarisation*. Spin physics can also be used to observe and study biological systems without intervening in them, through *e.g. in-vivo NMR spectroscopy*.

Unfortunately, some limitations to MRI, which should be resolvable, remain economical viability and physical constraints, *e.g.* due to patient size.

[2] During the late 2000s and 2010s, there were several reports by doctors and patients about patients that had been referred to local zoos in order to be able to receive MRI images. More information can be found in Ref. [19].

References

[1] G. E. Uhlenbeck *et al.*, 'Ersetzung der Hypothese vom unmechanischen Zwang durch eine Forderung bezüglich des inneren Verhaltens jedes einzelnen Elektrons', Nov. 1925.

[2] R. W. Brown *et al.*, *Magnetic resonance imaging: Physical principles and sequence design*. Wiley Blackwell, 2014.

[3] I. Duck *et al.*, *Pauli and the spin-statistics theorem*. World Scientific, 1998.

[4] J. Denck, Machine learning-based workflow enhancements in magnetic resonance imaging, 2022.

[5] T. C. Pochapsky *et al.*, *NMR for physical and biological scientists*. Garland Science, 29th Nov. 2019.

[6] D. W. McRobbie *et al.*, *MRI from picture to proton*. Cambridge University Press, 2017.

[7] C. Türk, Spin in quantum physics general theory and application on 'the proton spin crisis', 2003.

[8] I. Kuprov, *Spin: From basic symmetries to quantum optimal control*. 2023.

[9] A. Medek *et al.*, 'Multiple-quantum magic-angle spinning NMR', J. Braz. Chem. Soc., 1999.

[10] L. Bond *et al.*, 'Evaluation of non-nuclear techniques for well logging: Final report', U.S. Department of Energy, 2011.

[11] D. Weishaupt, *How does MRI work?* Springer-Verlag, 2008.

[12] W. Schlegel *et al.*, Eds., *Medizinische Physik: Grundlagen – Bildgebung – Therapie – Technik*, 2018.

[13] M. Levitt, *Spin dynamics*. 2008.

[14] D. Weishaupt *et al.*, *Wie funktioniert MRI?* Springer-Verlag, 2014.

[15] H. Haynes *et al.*, 'The emergence of magnetic resonance imaging (MRI) for 3d analysis of sediment beds', in Dec. 2013.

[16] "NMR principles," `https://chimactiv.agroparistech.fr/en/bases/rmn/theorie/3`, accessed: 12/01/2024.

[17] D. A. Pollacco, Magnetic resonance imaging, 2016.

[18] "No longer available," `https://www.greenriverspine.org/`, accessed: 12/01/2024.

[19] A. A. Ginde *et al.*, 'The challenge of CT and MRI imaging of obese individuals who present to the emergency department: A national survey', Nov. 2008.

[20] H. M. Gach *et al.*, 'MRI safety risks in the obese: The case of the disposable lighter stored in the pannus', 15th Mar. 2019.